AGU PUBLICATIONS

Geophysical Research Letters

RESEARCH LETTER
10.1002/2016GL070280

Key Points:
- ULF wave modulation of pitch angle distributions of both electrons and protons and chorus intensity occurs deep in the magnetosphere
- This ULF wave shows signatures of fundamental poloidal mode of field line resonance and mirror wave nature
- Linear growth rate calculation supports instability below 0.3 f_{ce}, while observed chorus at higher frequency requires nonlinear mechanisms

Correspondence to:
Z. Xia,
Zhiyang.Xia@utdallas.edu

Citation:
Xia, Z., L. Chen, L. Dai, S. G. Claudepierre, A. A. Chan, A. R. Soto-Chavez, and G. D. Reeves (2016), Modulation of chorus intensity by ULF waves deep in the inner magnetosphere, *Geophys. Res. Lett.*, *43*, 9444–9452, doi:10.1002/2016GL070280.

Received 1 JUL 2016
Accepted 29 AUG 2016
Accepted article online 5 SEP 2016
Published online 28 SEP 2016

©2016. American Geophysical Union. All Rights Reserved.

Modulation of chorus intensity by ULF waves deep in the inner magnetosphere

Zhiyang Xia[1], Lunjin Chen[1], Lei Dai[2], Seth G. Claudepierre[3], Anthony A. Chan[4], A. R. Soto-Chavez[5], and G. D. Reeves[6]

[1]Department of Physics, University of Texas at Dallas, Richardson, Texas, USA, [2]State Key Laboratory of Space Weather, National Space Science Center, Chinese Academy of Sciences, Beijing, China, [3]Space Science Department, Aerospace Corporation, El Segundo, California, USA, [4]Department of Physics and Astronomy, William Marsh Rice University, Houston, Texas, USA, [5]Center for Solar-Terrestrial Research, New Jersey Institute of Technology, Newark, New Jersey, USA, [6]Space Science and Applications Group, Los Alamos National Laboratory, Los Alamos, New Mexico, USA

Abstract Previous studies have shown that chorus wave intensity can be modulated by Pc4-Pc5 compressional ULF waves. In this study, we present Van Allen Probes observation of ULF wave modulating chorus wave intensity, which occurred deep in the magnetosphere. The ULF wave shows fundamental poloidal mode signature and mirror mode compressional nature. The observed ULF wave can modulate not only the chorus wave intensity but also the distribution of both protons and electrons. Linear growth rate analysis shows consistence with observed chorus intensity variation at low frequency ($f < \sim 0.3\, f_{ce}$), but cannot account for the observed higher-frequency chorus waves, including the upper band chorus waves. This suggests the chorus waves at higher-frequency ranges require nonlinear mechanisms. In addition, we use combined observations of Radiation Belt Storm Probes (RBSP) A and B to verify that the ULF wave event is spatially local and does not last long.

1. Introduction

Chorus emission is one of the whistler-mode waves occurring in the Earth's magnetosphere in the typical frequency range between 0.1 to 0.8 f_{ce} (f_{ce} is the equatorial electron gyrofrequency) [*Tsurutani and Smith*, 1977; *Koons and Roeder*, 1990]. Chorus usually occurs in two separate frequency bands within the frequency range mentioned above, one is 0.1 to 0.5 f_{ce} (the lower band) and the other is above 0.5 f_{ce} (the upper band) [*Tsurutani and Smith*, 1974; *Burtis and Helliwell*, 1976, 1969]. The chorus waves originate near the geomagnetic equator outside the plasmapause [*LeDocq et al.*, 1998; *Lauben et al.*, 2002; *Santolík et al.*, 2003] due to the cyclotron resonant interaction with anisotropic plasma sheet electrons injected into the inner magnetosphere in the 10–100 keV energy range [*Li et al.*, 2009, 2010]. It is generally believed that the intensity and occurrence of chorus are associated with geomagnetic activity, and most of the chorus waves take place during geomagnetic disturbances [*Tsurutani and Smith*, 1974; *Meredith et al.*, 2001, 2003a, 2003b; *Miyoshi et al.*, 2003; *Lyons et al.*, 2005].

Ultralow frequency (ULF) oscillation of geomagnetic field lines can be excited, in general, by sources external or internal to the magnetosphere. Solar wind dynamic pressure fluctuations can be a substantial source for magnetosphere ULF wave power [*Kessel*, 2008; *Takahashi and Ukhorskiy*, 2007; *Dai et al.*, 2015]. ULF waves generated by external sources are compressional waves of fast-mode nature and characterized by a global-scale azimuthal wavelength (or small azimuthal wave number). In contrast, internal instabilities excite more localized ULF waves with a small azimuthal wavelength. The instabilities could be drift or drift-bounce instability [*Southwood*, 1976; *Dai et al.*, 2013] or drift mirror instability [*Cheng and Lin*, 1987; *Chen and Hasegawa*, 1991]. These two instabilities, which generally are coupled, are more effective in low-β and high-β plasma, respectively.

The time scale of the chorus elements is about a tenth to a few tenths of seconds [*Santolík et al.*, 2003]. Previous studies have shown that the intensity of chorus waves can be modulated by ULF waves on a few seconds to a few minutes timescale [e.g., *Tixier and Cornilleau-Wehrlin*, 1986; *Manninen et al.*, 2010]. *Li et al.* [2011] have analyzed several events where the intensity of chorus waves can be modulated by the compressional Pc4-Pc5 ULF waves with antiphase correlation between the magnetic field and electron density which

is inferred from spacecraft potential. They found that the chorus intensity enhances with increased electron density and with depletion of magnetic field and is weaker when the electron density reaches its valley and magnetic field reaches its crest. This kind of modulations occurs in the large L shell area (8 to 12) where external solar wind sources are likely the driver. In this paper, we present Van Allen Probes observation of a modulation of chorus wave intensity by ULF waves event, which is excited internally deep in the magnetosphere during a strong geomagnetic storm and also shows many other modulating signatures. The Van Allen Probes (formerly known as the Radiation Belt Storm Probes (RBSP)) [*Mauk et al.*, 2013] are capable of detecting the upper hybrid resonance line, which enables calibration of density inferred from spacecraft potential and better captures the density variation associated with ULF waves. The organization of this paper is as follows: Van Allen Probes instrumentation is described in section 2, followed by the observation and the interpretation of the modulation event in sections 3 and 4. Conclusions and discussion are given in section 5.

2. Van Allen Probes Instrumentation

The Van Allen Probes are two robotic spacecrafts equipped with identical instruments and move on nearly identical orbits near the Earth's equatorial plane.

The Electric and Magnetic Field Instrument Suite and Integrated Science (EMFISIS) [*Kletzing et al.*, 2013] carries two sensors, a triaxial fluxgate magnetometer (MAG) and a triaxial AC magnetic search coil magnetometer, which provide comprehensive wave magnetic field measurements in the frequency range of 10 Hz to 400 kHz. The Electric Field and Waves Suite (EFW) [*Wygant et al.*, 2013] is used to study the electric fields in near-Earth space; it provides not only the components of electric field but also a spacecraft potential estimate covering cold plasma densities of 0.1 to 100 cm^{-3}. The empirical density-potential formula has been calibrated according to EMFISIS upper hybrid resonance (UHR) lines, which provides more accurate characterization of density variation associated with ULF waves than previous studies [e.g., *Li et al.*, 2011] using spacecraft potential alone. The Energetic Particle, Composition, and Thermal Plasma Suite (ECT) [*Spence et al.*, 2013] is made up of three separate components: Helium, Oxygen, Proton, and Electron (HOPE) for the energy range 0.001 to 50 keV [*Funsten et al.*, 2013]; Magnetic Electron Ion Spectrometer (MagEIS), for three different particle populations (ring current electrons ~20 to ~200 keV and radiation belt electrons >~200 keV to ~3 MeV, ring current protons, and radiation belt protons 60 keV to 1 MeV) [*Blake et al.*, 2013]; and the Relativistic Electron Proton Telescope for the proton energy range ~17 to >100 MeV and electron energy range ~1.6 to >~19 MeV [*Baker et al.*, 2013].

3. ULF Wave Observation

The ULF event of interest observed by Van Allen Probes occurs during a storm between 13:40UT and 14:30UT on 6 July 2013. Figures 1a–1g show the variations of geomagnetic indexes and solar wind parameters over 3 days of 5–8 July. The red vertical line labeled t_0 marks the time when RBSP B detected the modulation event, and the green and blue vertical lines labeled t_- and t_+, respectively, are the last and next time periods when RBSP A passes near the location where the modulation event was observed at t_0. Figures 1h and 1i show the orbits of the RBSP A and RBSP B projected on the equator plane along the field line in solar magnetic (SM) coordinate. The projection of the RBSP B orbit in t_0 is around $x = -4\,R_e$, $y = 3\,R_e$ in the SM equatorial plane, while RBSP A traveled nearby ($x = 1\,R_e$, $y = 3\,R_e$). RBSP A moved through the event location at the two nearest time periods, about 09:24 UT to 10:14 UT (denoted as t_-) and 17:50 UT to 18:40 UT (denoted as t_+) on 6 July 2013, both of which are about 4 h away from t_0. We note that all the three time periods are within the storm period which lasts for a whole day on 6 July. In these three time periods, the *Kp*, *AE*, and *Dst* indexes all have high absolute values; the number density, and velocity of solar wind remain nearly constant at about 10 cm^{-3} and 340 km/s; and the interplanetary magnetic field B_z component remains negative (as low as −10 nT) over the entire day of 6 July, leading to a moderate geomagnetic storm with *Dst* minimum ~−80 nT.

This geomagnetic storm results in the generation of ULF waves deep inside the magnetosphere ($L \sim 5$) and the corresponding modulation of chorus wave intensity, which will be the topics of this study. Figure 2 focuses on the modulation event observed from RBSP B. Figures 2a and 2b show the variations of the plasma density from spacecraft potential with calibration by the UHR line from EMFISIS and the three components of magnetic field fluctuation in the mean magnetic field aligned coordinate, radial component B_r, azimuthal component B_a, and parallel component B_p. The magnetic field fluctuation data are obtained from the original MAG magnetic field data after detrending with a smooth time window of 300 s. From Figures 2a and 2b,

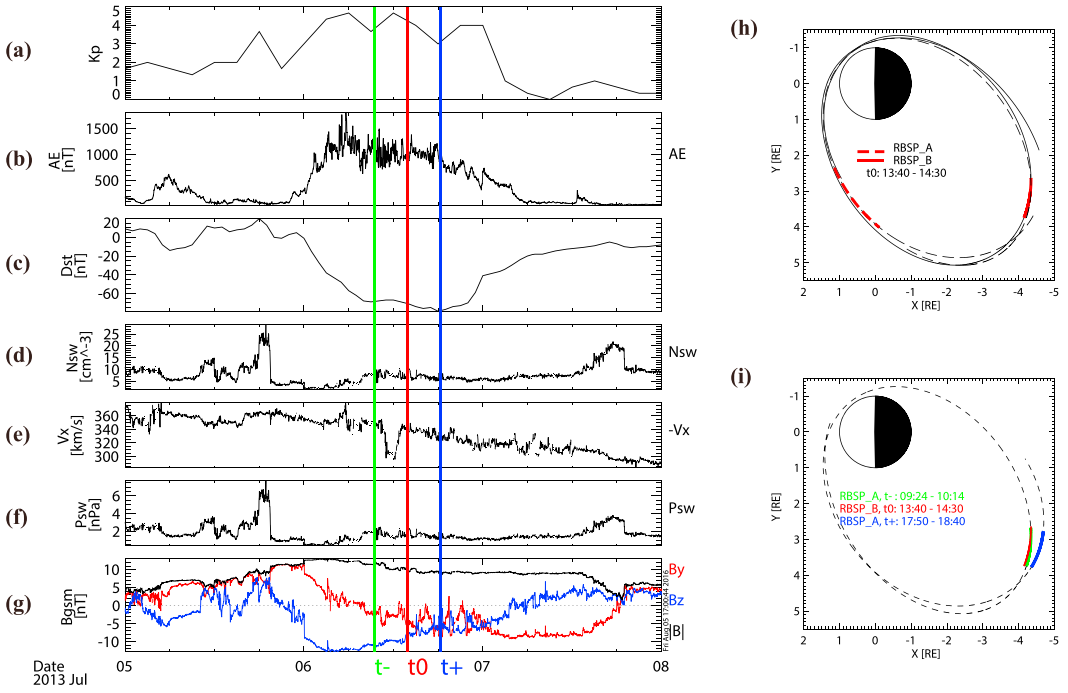

Figure 1. Overview of geomagnetic indexes and solar wind parameters from OMNI for the modulation event. (a) *Kp*, (b) *AE*, (c) *Dst* index, (d) the solar wind density, (e) velocity, (f) pressure, and (g) magnetic field through the period of the storm event. The green, red and blue vertical lines denote the times t_-, t_0, and t_+, respectively (see text). (h and i) The orbits projected on the equator plane along a dipole field line for the satellites RBSP A and RBSP B. Red lines in Figure 1h highlight satellite orbits near t_0, and green, red, and blue lines in Figure 1i highlight the orbits near t_-, t_0, and t_+.

we can clearly see the variation of density is out of phase with the variation of B_p, while the B_a and B_r fluctuations are weaker comparing to the B_p fluctuation, indicating that this ULF wave is a mostly compressional wave with rather large amplitude B_p up to 10 nT. The period of the variation is about 150 s, which tells us that this is a Pc4-Pc5 ULF wave. The observed ULF wave is consistent with the wave generation through a drift mirror instability. In a pure drift mirror mode, $B_p >> B_r$ [*Chen and Hasegawa*, 1991], and in our event, the compressional component B_p is about 2–3 times larger than the poloidal component B_r (Figure 2b). Additional consistent characteristics of the drift mirror mode [*Hasegawa*, 1969] include the followings: (1) the variation of the magnetic pressure and the variation of the plasma pressure are out of phase and comparable (Figure 2c), (2) the variation amplitude of perpendicular pressure is greater than that of parallel pressure (Figure 2c), (3) plasma beta is large (β_{perp} up to 2) and (4) the electric field perturbation at the ULF wave frequency is rather weak (not shown). In addition, the pressure of electrons exhibits similar characteristics but with much smaller variations (not shown) than that of protons (Figure 2c). Such large β (β_{perp} up to 2) closely approaches, but not exceeding, that required by the linear instability of drift mirror mode expressed by the formula (24) in *Hasegawa* [1969]. Possible reasons for this are the relaxation by nonlinear saturation due to the large magnetic amplitude and the consideration of HOPE measurement (<∼ 50 keV) only.

Because of the presence of finite radial magnetic field perturbation (B_r), we also check frequencies for pure poloidal modes. We solve for the eigenperiods in a dipole magentic field using equation (6) of *Cummings et al.* [1969] with $L = 5.5$ (observation location), and adopting latitudinal dependence of mass density along a field line, $\rho(\lambda) = M_i N_{eq} \cos^m \lambda$, where observed equatorial electron density $N_{eq} = 10\ cm^{-3}$, λ is the magnetic latitude, m is the density index, and M_i is the average ion mass. Figure 3 shows calculation of fundamental, second harmonic, and third harmonic poloidal mode periods as a function of M_i from 1 (all H^+ ions) to 16 (all O^+ ions) and a function of m over a typical range from 1 to 6. The observed period (150 s) is close to the fundamental period of the poloidal mode with $M_i \sim 1.5$, with little dependence on the m value. HOPE data provide H^+, He^+, and O^+ density measurements in the energy range above 30 eV, which are about 1.75, 0.07, and 0.35 cm^{-3}, respectively, over the event period. Based on those ion densities, M_i is about 3.5. Because thermal H^+ ions (∼ eV) tend to be the dominant ion species, the value of M_i can be lower when taking in account ion populations below 30 eV, which is not available due to positive spacecraft charge. The second harmonic period

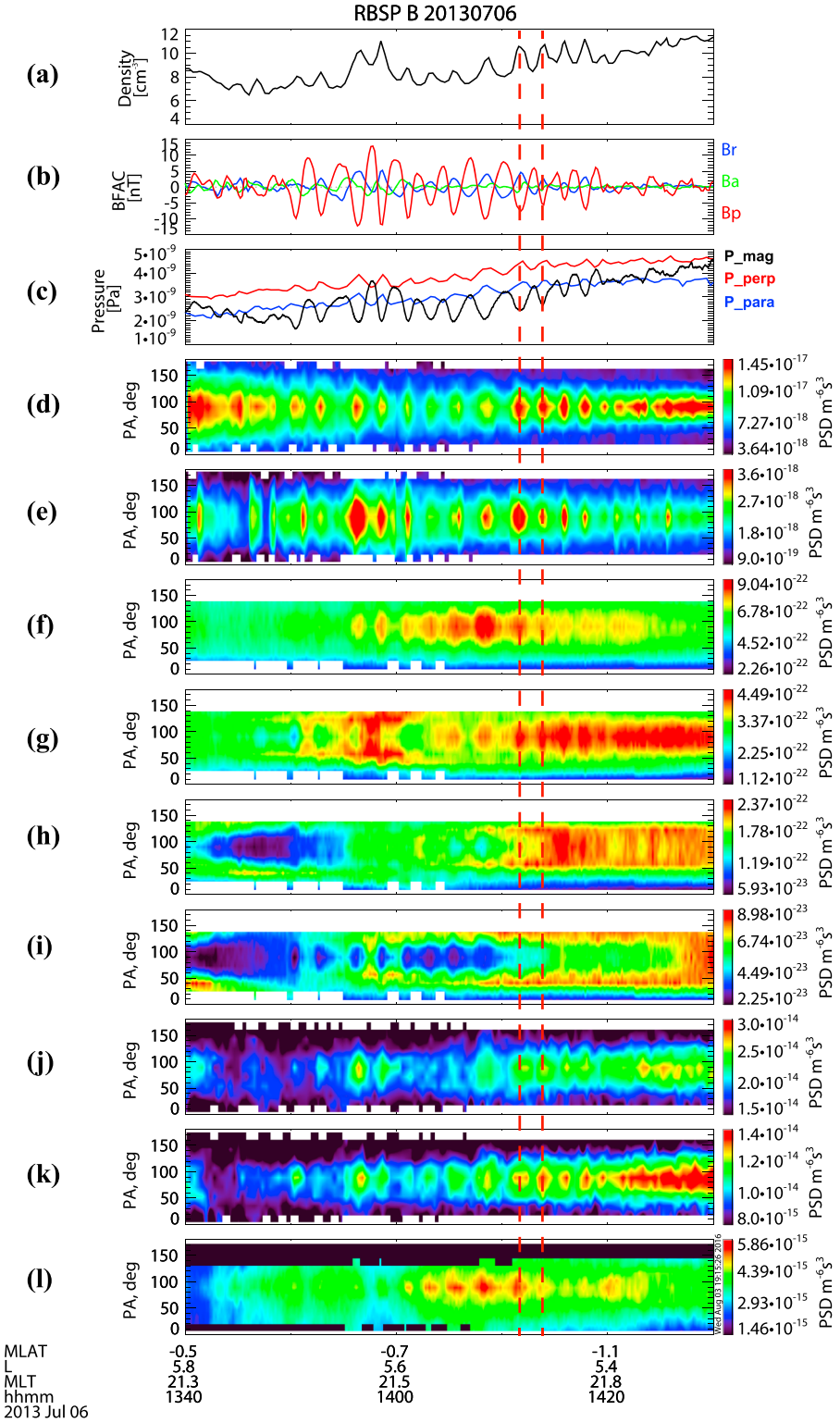

Figure 2. Relationship between particle distribution and ULF waves from RBSP B observations: (a) the variation of plasma density from EFW s/c potential; (b) the variation of three components of magnetic field; (c) the variations of the magnetic pressure (black) and the perpendicular (red) and parallel (blue) pressures of protons; pitch angle distribution of electron phase space density at energies (d) 1046.67 eV, (e) 2620.96 eV, (f) 31.9 keV, (g) 54.4 keV, (h) 75.1 keV, and (i) 101.6 keV; and pitch angle distribution of proton phase space density at energies (j) 9631.9 eV, (k) 15,236.9 eV, and (l) 62.74 keV. The two vertical red-dotted lines denotes ULF wave phases corresponding to plasma density peaks.

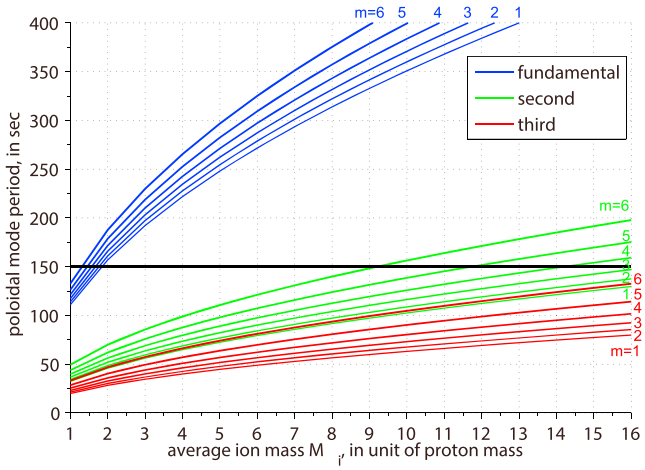

Figure 3. Calculation of poloidal mode periods as a function of average ion mass and field-aligned density index *m*. Fundamental, second harmonic, and third harmonic poloidal modes are denoted by blue, green, and red lines, respectively. The horizontal black line denotes the period of the observed ULF wave. The numbers next to the lines represent the value of the density index *m* from 1 to 6.

is much shorter than the fundamental period and can match the observed period for a high value of $m = 6$ if nearly half ions are O^+, which is unlikely for our case. Comparison is even worse for second harmonic period with lower *m* and also for the period of the third harmonic. If it were second or third harmonic, it would need an unrealistically high-O^+ concentration (requiring dominant ions should be O^+ ions). We conclude that the observed ULF wave is a coupling between a drift mirror and fundamental poloidal mode.

The observed ULF wave closely modulates both electron and proton pitch angle distributions. Figures 2d–2i show electron phase space density (PSD) versus pitch angle at energy channels 1047 and 2621 eV from the ECT-HOPE instrument and 32, 54, 75, and 102 keV from the ECT-MagEIS instrument. Figures 2j–2l show proton PSD at energy channels 9632 and 15,237 eV from ECT-HOPE and 62.74 keV from ECT-MagEIS. The distributions of both electrons (Figures 2d–2f) and protons (Figures 2j–2l) are modulated by the ULF wave in a similar fashion. The phase space densities of both protons and electrons increase especially near 90° pitch angle when the plasma density reaches its crest and B_p reaches its valley, while the phase space densities decrease at the plasma density valley and B_p crest. This feature is highlighted by the area between the two vertical red-dotted lines. After checking electron and proton distributions at other energies we note that the electron energy ranging from 0.2 to 54 keV and the proton energy ranging from 5 to 63 keV are involved in this kind of ULF modulation and that these modulation signatures are not present clearly beyond these two energy ranges for electrons and ions respectively. Moreover, over a higher electron energy range 54.4 keV–101 kev (Figures 2g–2i), the electron distribution shows a different response at B_p valleys where electron PSD at 90° tends to reduce and peak PSD goes to lower pitch angle. The transition of electron PSD at 90° from out-of-phase with B_p to in-phase occurs over a relatively narrow energy range of 54–75 keV (Figures 2g and 2h). Note that there is no clear signature of such a transition in the response of proton distribution in our event. The phase-jump transition of electron PSD reported here is somewhat different from the transition of electron energy in drift-resonance response to ULF wave phase reported by *Claudepierre et al.* [2013], where modulated electron flux variation shows a clear energy of peak variation amplitude and the phase difference between electron flux variation and the ULF wave phase varies slowly as a function of energy. If one assumes the phase-jump transition reported by our event is another kind of electron drift-resonance signature, then it can be estimated, using $f = nf_d$, that the ULF wave azimuthal number $n \sim 56$, where wave frequency $f = 1/150$ Hz and drift frequency f_d is calculated for electrons at energy 60 keV and equatorial pitch angle 90° at $L = 5.5$. The value of *n* is a reasonable value for an internally or kinetically excited magnetohydrodynamic wave. Further investigation of such electron behavior is beyond the scope of our current study.

4. Chorus Wave Observation

Figure 4 shows the relationship between ULF and VLF waves. Figures 4a and 4b show the B_p variation and the electron spectrum of 1046.67 eV, respectively, which are the same as Figures 2b and 2d. Figures 4c–4f

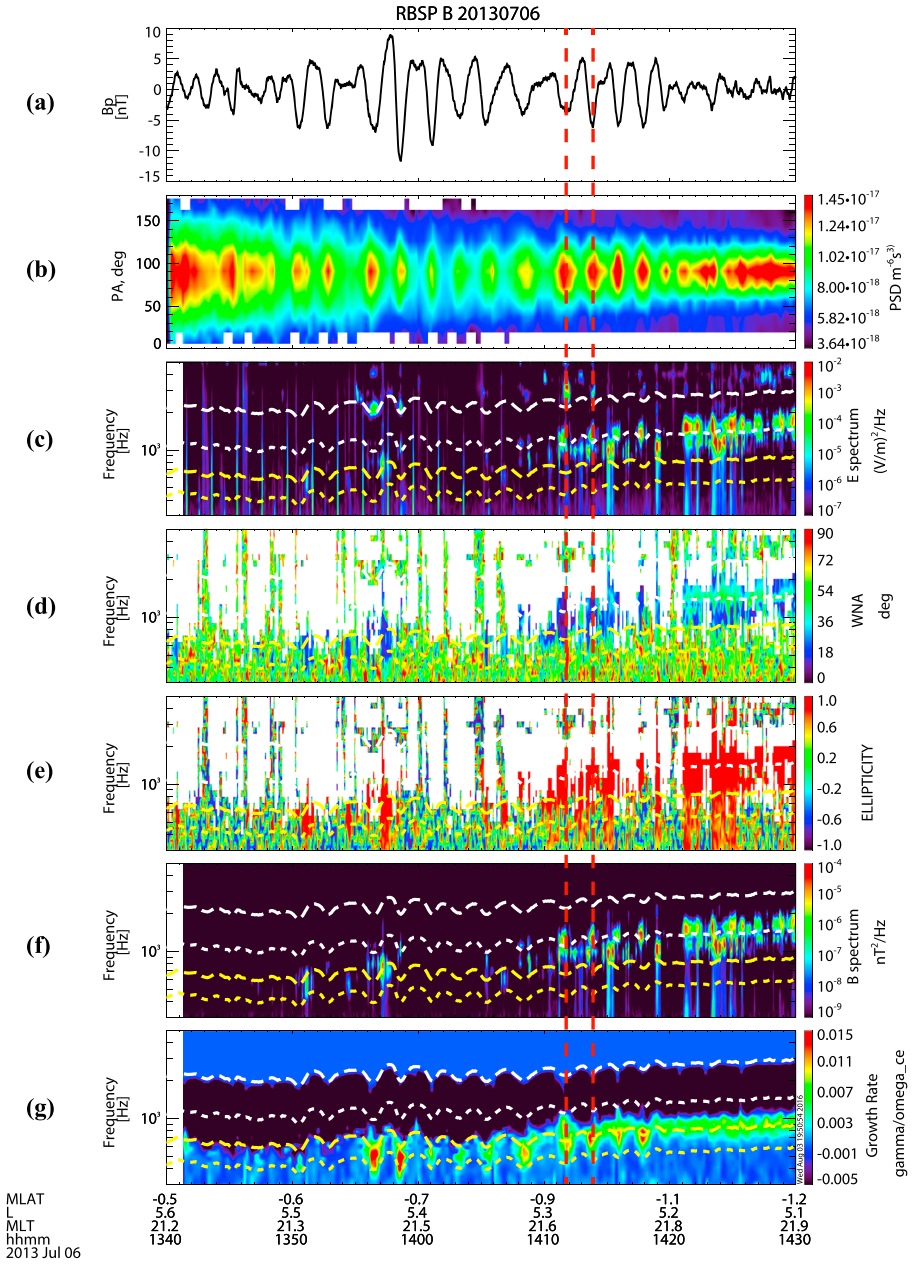

Figure 4. Relationship of magnetic perturbation and VLF chorus waves: (a) the parallel magnetic field fluctuation (same as the red line in Figure 2b), (b) pitch angle distribution of electron phase space density at energy 1046.67 eV, (c) power spectrum density of wave electric field, (d) wave normal angle, (e) ellipticity, (f) wave magnetic field, and (g) the linear growth rate calculated. The white long dashed and short dashed lines represent f_{ce} and 0.5 f_{ce}, respectively, and the yellow long dashed and short dashed lines represent 0.3 f_{ce} and 0.2 f_{ce}, respectively.

show, respectively, the spectras of wave electric field, wave normal angle, ellipticity, and wave magnetic field from the EMFISIS measurement. At the valley of B_p and the crest of the electron phase space density, there exists intense chorus wave magnetic and electric power below and above 0.5 f_{ce} with about 0° wave normal angle and ellipticity near 1. Chorus waves turn on and off quasiperiodically over 14:10 UT to 14:20 UT with time period close to the period of the ULF waves. Close examination shows that both upper and lower band chorus waves are intensified at the valleys of B_p (showed by the two vertical lines in Figure 4) corresponding to the increase of electron phase space density (Figure 4b), while chorus waves diminish at the crests of B_p. This relation is in part similar to the modulation event *Li et al.* [2011] found, but our event occurred deep

inside the magnetosphere where ULF wave is internally excited by ring current population. The set of ULF waves, VLF waves, and particle distributions provides strong support that ULF waves can modulate chorus wave intensity and that the variation of the electron distribution causes the chorus waves to turn on and off. We should make following two notes. First, there is no clear chorus modulation prior to 14:10, although with variation of electron phase space density and linear growth rate. Second, some lower band chorus bursts (~14:14 and 14:19) can occurs closer to density valleys (B_p crests) rather than density crests (B_p valleys). Those inconsistencies might be attributed to two physical processes other than local linear growth. First, nonlinear wave growth shows dependence on magnetic field topology, in particular the field-aligned variation of the ambient magnetic field [*Tao*, 2014; *Katoh and Omura*, 2011], which varies with ULF wave phases and depends on field line resonance (FLR) eigenmode structures. Second, propagation effect may also lead to wave refraction toward both lower and higher-density ducts [*Katoh*, 2014]. This is especially true for fine-scale density variation associated with ULF wave of high azimuthal wave number.

Variations of electron pitch angle distribution are the response to ULF waves, rather than the consequence of chorus waves scattering; this is supported by the following observations: (1) protons respond in similar fashion to electrons while chorus can not effectively scatter protons and (2) the presence of the electron variations already began at about 13:50 UT (Figures 2d–2f), before the chorus wave variation (14:10 UT to 14:20 UT). Based on parameters typical for this observation event, electron minimum gyroresonant energy for the lower band chorus is several keV (not shown) and even lower for the upper band chorus. Thus, the phase jump near 50 keV mentioned above is unlikely a consequence of gyroresonance interaction.

To test the idea that electron variation is indeed responsible for chorus wave generation, linear instability analysis based on observed plasma condition is performed. The linear growth rate of whistler-mode waves can be calculated by using the linear theory equation [*Kennel and Petschek*, 1966] and using measured parameters, including plasma density (calibrated from upper hybrid resonant lines), background magnetic field, and observed electron velocity distribution from the HOPE instrument. These measurement from Van Allen Probes provides unambiguous parameters to make possible a definite test of the linear theory.

Figure 4g shows the growth rate as a function of time and frequency for parallel propagation. We also did calculations for other wave normal angles up to the whistler-mode resonance cone angle and found that the growth rate maximizes for parallel propagation. The result of linear growth rate analysis shows the coincidence between the maximum of the growth rate and the occurrence of intense chorus waves at $<\sim 0.3\, f_{ce}$, which is consistent with the variation of electron flux changing the plasma instability and thus generating the chorus waves. However, the frequency range of the growth rate enhancement and that of the chorus wave do not always match, especially for higher-frequency portions. The growth rate above $0.5\, f_{ce}$ is very low all the time. This indicates that higher-frequency chorus waves, including upper band chorus, should be due to a mechanism other than linear instability.

With twin Van Allen Probes we can infer whether this modulation is local or global by examining two simultaneous observations and estimate its time duration. Temporal and spatial scales of this modulation event are checked using the Van Allen Probes pair. We checked the RBSP A data at t_0, t_-, and t_+ (indicated by Figure 1). No clear signatures of ULF waves and particle and chorus waves modulation are found at the $t_\pm$ intervals, indicating that the event we analyzed only lasts no longer than a few hours. We also check RBSP A observation at t_0, which is about $\sim 2-3\, R_E$ from RBSP B, and find no clear signature of ULF wave activity, either suggesting that the event captured by RBSP B is not a global ULF wave. Such spatially local and temporal natures are consistent with internally excited ULF waves. This localized phenomena, occurring at premidnight during the main phase, might be associated with the westward edge of partial ring current (indicated by Figure 2c where thermal pressure increases with magnetic local time) developed from fresh injection.

5. Conclusions and Discussion

In summary, in this study we present an event of chorus modulation by ULF waves deep inside the magnetosphere. Using Van Allen Probes observations, we analyzed the relationships between the intensity of chorus wave and the magnitude of plasma density, magnetic field variation and the distribution of electrons and protons. Moreover, we also calculate the linear whistler-mode growth rate to help understand the mechanism

of the modulation of chorus waves. Then we combined the observations of both RBSP A and B to estimate the temporal and spatial scales of this kind of modulation. Our conclusions are summarized as follows:

1. An event of ULF wave modulation of pitch angle distributions of both electrons and protons is reported deep in the magnetosphere, which occurs during a geomagnetic storm with long lasting negative interplanetary magnetic field B_z.
2. This ULF wave shows signatures of fundamental poloidal mode of field line resonance and mirror wave nature. At the crest of plasma density and the valley of the compressional component of the wave magnetic field, the phase space density near pitch angle 90° increases for protons over 5–63 keV and for electrons over 0.2–54 keV, while in contrast, the electron pitch angle distributions are notably different (strongly field aligned) at the higher energies above 60 keV.
3. The ULF wave tends to modulate the electron distribution and thus the intensity of whistler-mode chorus waves; consistency with the linear growth rate analysis of the observed electron distribution for whistler mode at low frequency ($<\sim 0.3\, f_{ce}$). The linear instability, however, cannot account for the observed chorus at higher frequency (including the upper band chorus).
4. This ULF wave and modulation phenomenon is spatially local and does not last long.

Many observed modulation signatures along with our quantitative analysis, allow us to sort out the physical processes behind the event. Here is our interpretation based on the observation and the analysis performed. A local and temporal ULF wave with antiphase correlation between plasma density and compressional magnetic field component is generated internally deep in the magnetosphere, probably through a drift mirror instability. Self-consistently, the generated ULF wave causes disturbances in both electron and ion pitch angle distributions, whose anisotropy enhances in the crests of plasma density. The enhanced electron pitch angle distribution leads to enhanced chorus wave intensity at the low-frequency range ($<\sim 0.3\, f_{ce}$). Some other nonlinear mechanisms further trigger the chorus wave generation at higher-frequency range, including the upper band chorus. This conclusion provides strong observational support for nonlinear chorus wave generation mechanism, where linear growth rate at lower frequency is required and higher-frequency chorus can be generated nonlinearly in the form of rising tone element [*Tao*, 2014; *Katoh and Omura*, 2011].

There are a variety of ULF waves, with or without plasma density variation, compressional, or transverse wave magnetic field component, which are generated by different free energy. Beside chorus waves, there are also other types of whistler-mode waves, such as plasmaspheric hiss or magnetosonic waves. *Breneman et al.* [2015] present an event of plasmaspheric hiss modulated by ULF waves over a global scale, leading to modulated electron precipitation. Likewise, the modulated chorus emission might lead to modulated electron precipitation, such as the formation of pulsating aurora [*Nishimura et al.*, 2010; *Jaynes et al.*, 2015]. General questions on ULF waves generation and their modulatory effect on VLF waves and electron precipitation are interesting and will be investigated with a continuing effort.

Acknowledgments
This research was supported by the NSF Geospace Environment Modeling grant AGS 1405041. A.A.C. would like to acknowledge the support of NASA grant NNX15AI93G and NNX14AN55G. We acknowledge Van Allen Probe teams for data usage. Data presented in the study are obtained from the NASA/SPDF website http://spdf.sci.gsfc.nasa.gov/pub/data/rbsp/. We also acknowledge NASA/GSFC's Space Physics Data Facility's OMNI data for the data of solar wind parameters and geomagnetic indexes.

References

Baker, D. N., et al. (2013), The relativistic electron-proton telescope (REPT) instrument on board the radiation belt storm probes (RBSP) spacecraft: Characterization of Earth's radiation belt high-energy particle populations, *Space Sci. Rev.*, *179*, 337–381, doi:10.1007/s11214-012-9950-9.

Blake, J. B., et al. (2013), The magnetic electron ion spectrometer (MagEIS) instruments aboard the radiation belt storm probes (RBSP) spacecraft, *Space Sci. Rev.*, *179*, 383–421, doi:10.1007/s11214-013-9991-8.

Breneman, A. W., et al. (2015), Global-scale coherence modulation of radiation-belt electron loss from plasmaspheric hiss, *Nature*, *523*, 193–195, doi:10.1038/nature14515.

Burtis, W. J., and R. A. Helliwell (1969), Banded chorus: A new type of VLF radiation observed in the magnetosphere by OGO 1 and OGO 3, *J. Geophys. Res.*, *74*, 3002, doi:10.1029/JA074i011p03002.

Burtis, W. J., and R. A. Helliwell (1976), Magnetospheric chorus—Occurrence patterns and normalized frequency, *Planet. Space Sci.*, *24*, 1007–1024, doi:10.1016/0032-0633(76)90119-7.

Chen, L., and A. Hasegawa (1991), Kinetic theory of geomagnetic pulsations: I—Internal excitations by energetic particles, *J. Geophys. Res.*, *96*, 1503–1512, doi:10.1029/90JA02346.

Cheng, C. Z., and C. S. Lin (1987), Eigenmode analysis of compressional waves in the magnetosphere, *J. Geophys. Res.*, *14*, 884–887, doi:10.1029/GL014i008p00884.

Claudepierre, S. G., et al. (2013), Van Allen Probes observation of localized drift resonance between poloidal mode ultra-low frequency waves and 60 keV electrons, *Geophys. Res. Lett.*, *40*, 4491–4497, doi:10.1002/grl.50901.

Cummings, W. D., R. J. O'Sullivan, and P. J. Coleman Jr. (1969), Standing Alfvén waves in the magnetosphere, *J. Geophys. Res.*, *74*, 778, doi:10.1029/JA074i003p00778.

Dai, L., et al. (2013), Excitation of poloidal standing Alfvén waves through drift resonance wave-particle interaction, *J. Geophys. Res.*, *40*, 4127–4132, doi:10.1002/grl.50800.

Dai, L., et al. (2015), Storm time occurrence and spatial distribution of Pc4 poloidal ULF waves in the inner magnetosphere: A Van Allen Probes statistical study, *J. Geophys. Res.*, *120*, 4748–4762, doi:10.1002/2015JA021134.

Funsten, H. O., et al. (2013), Helium, Oxygen, Proton, and Electron (HOPE) mass spectrometer for the Radiation Belt Storm Probes mission, *Space Sci. Rev.*, *179*, 423–484, doi:10.1007/s11214-013-9968-7.
Hasegawa, A. (1969), Drift mirror instability of the magnetosphere, *Phys. Fluids*, *12*, 2642–2650, doi:10.1063/1.1692407.
Jaynes, A. N., et al. (2015), Correlated Pc4-5 ULF waves, whistler-mode chorus, and pulsating aurora observed by the Van Allen Probes and ground-based systems, *J. Geophys. Res.*, *120*, 8749–8761, doi:10.1002/2015JA021380.
Katoh, Y. (2014), A simulation study of the propagation of whistler-mode chorus in the Earth's inner magnetosphere, *Earth, Planets, and Space*, *66*, 6, doi:10.1186/1880-5981-66-6.
Katoh, Y., and Y. Omura (2011), Amplitude dependence of frequency sweep rates of whistler mode chorus emissions, *J. Geophys. Res.*, *116*, A07201, doi:10.1029/2011JA016496.
Kennel, C. F., and H. E. Petschek (1966), Limit on stably trapped particle fluxes, *J. Geophys. Res.*, *71*, 1.
Kessel, R. L. (2008), Solar wind excitation of Pc5 fluctuations in the magnetosphere and on the ground, *J. Geophys. Res.*, *113*, A04202, doi:10.1029/2007JA012255.
Kletzing, C. A., et al. (2013), The Electric and Magnetic Field Instrument Suite and Integrated Science (EMFISIS) on RBSP, *Space Sci. Rev.*, *179*, 127–181, doi:10.1007/s11214-013-9993-6.
Koons, H. C., and J. L. Roeder (1990), A survey of equatorial magnetospheric wave activity between 5 and 8 R(E), *Planet. Space Sci.*, *38*, 1335–1341, doi:10.1016/0032-0633(90)90136-E.
Lauben, D. S., et al. (2002), Source characteristics of ELF/VLF chorus, *J. Geophys. Res.*, *107*(A12), 1429, doi:10.1029/2000JA003019.
LeDocq, M. J., D. A. Gurnett, and G. B. Hospodarsky (1998), Chorus source locations from VLF Poynting flux measurements with the polar spacecraft, *Geophys. Res. Lett.*, *25*, 4063, doi:10.1029/1998GL900071.
Li, W., et al. (2009), Evaluation of whistler-mode chorus intensification on the nightside during an injection event observed on the THEMIS spacecraft, *J. Geophys. Res.*, *114*, A00C14, doi:10.1029/2008JA013554.
Li, W., et al. (2010), THEMIS analysis of observed equatorial electron distributions responsible for the chorus excitation, *J. Geophys. Res.*, *115*, A00F11, doi:10.1029/2009JA014845.
Li, W., et al. (2011), Modulation of whistler mode chorus waves: 1. Role of compressional Pc4-5 pulsations, *J. Geophys. Res.*, *116*, A06205, doi:10.1029/2010JA016312.
Lyons, L. R., et al. (2005), Solar wind-magnetosphere coupling leading to relativistic electron energization during high-speed streams, *J. Geophys. Res.*, *110*, A11202, doi:10.1029/2005JA011254.
Manninen, J., N. G. Kleimenova, O. V. Kozyreva, and T. Turunen (2010), Pc5 geomagnetic pulsations, pulsating particle precipitation, and VLF chorus: Case study on 24 November 2006, *J. Geophys. Res.*, *115*, A00F14, doi:10.1029/2009JA014837.
Mauk, B. H., et al. (2013), Science objectives and rationale for the Radiation Belt Storm Probes mission, *Space Sci. Rev.*, *179*, 3–27, doi:10.1007/s11214-012-9908-y.
Meredith, N. P., R. B. Horne, and R. R. Anderson (2001), Substorm dependence of chorus amplitudes: Implications for the acceleration of electrons to relativistic energies, *J. Geophys. Res.*, *106*, 13,165–13,178, doi:10.1029/2000JA900156.
Meredith, N. P., et al. (2003a), Favored regions for chorus-driven electron acceleration to relativistic energies in the Earth's outer radiation belt, *Geophys. Res. Lett.*, *30*, 1871, doi:10.1029/2003GL017698.
Meredith, N. P., et al. (2003b), Evidence for chorus-driven electron acceleration to relativistic energies from a survey of geomagnetically disturbed periods, *J. Geophys. Res.*, *108*, 1248, doi:10.1029/2002JA009764.
Miyoshi, Y., et al. (2003), Rebuilding process of the outer radiation belt during the 3 November 1993 magnetic storm: NOAA and Exos-D observations, *J. Geophys. Res.*, *108*, 1004, doi:10.1029/2001JA007542.
Nishimura, Y., et al. (2010), Identifying the driver of pulsating aurora, *Science*, *330*, 81, doi:10.1126/science.1193186.
Santolík, O., et al. (2003), Spatio-temporal structure of storm-time chorus, *J. Geophys. Res.*, *108*, 1278, doi:10.1029/2002JA009791.
Southwood, D. J. (1976), A general approach to low-frequency instability in the ring current plasma, *J. Geophys. Res.*, *81*, 3340–3348, doi:10.1029/JA081i019p03340.
Spence, H. E., et al. (2013), Science goals and overview of the Radiation Belt Storm Probes (RBSP) energetic particle, composition, and thermal plasma (ECT) suite on NASA's Van Allen Probes mission, *Space Sci. Rev.*, *179*, 311–336, doi:10.1007/s11214-013-0007-5.
Takahashi, K., and A. Y. Ukhorskiy (2007), Solar wind control of Pc5 pulsation power at geosynchronous orbit, *J. Geophys. Res.*, *112*, A11205, doi:10.1029/2007JA012483.
Tao, X. (2014), A numerical study of chorus generation and the related variation of wave intensity using the DAWN code, *J. Geophys. Res.*, *119*, 3362–3372, doi:10.1002/2014JA019820.
Tixier, M., and N. Cornilleau-Wehrlin (1986), How are the VLF quasi-periodic emissions controlled by harmonics of field line oscillations? The results of a comparison between ground and GEOS satellites measurements, *J. Geophys. Res.*, *91*, 6899–6919, doi:10.1029/JA091iA06p06899.
Tsurutani, B. T., and E. J. Smith (1974), Postmidnight chorus: A substorm phenomenon, *J. Geophys. Res.*, *79*, 118–127, doi:10.1029/JA079i001p00118.
Tsurutani, B. T., and E. J. Smith (1977), Two types of magnetospheric ELF chorus and their substorm dependences, *J. Geophys. Res.*, *82*, 5112–5128, doi:10.1029/JA082i032p05112.
Wygant, J. R., et al. (2013), The Electric Field and Waves instruments on the Radiation Belt Storm Probes Mission, *Space Sci. Rev.*, *179*, 183–220, doi:10.1007/s11214-013-0013-7.